Au Nanosheets

DOI: 10.1002/anie.201304122

Self-Assembly of Au_{15} into Single-Cluster-Thick Sheets at the Interface of Two Miscible High-Boiling Solvents**

Zhennan Wu, Chunwei Dong, Yanchun Li, Hongxia Hao, Hao Zhang, Zhongyuan Lu,* and Bai Yang*

Exploring new methods to create self-assembled monolayers of nanostructures is fundamental both for understanding the microscopic interactions and creating low-dimensional quantum-confined materials.[1–3] Despite numerous reports of two-dimensional self-assembly of nanoparticles composed of hundreds of atoms, limited success has been achieved when employing much smaller nanoclusters (NCs).[4–16] As to NCs, the thermal fluctuation energy of the surroundings is comparable to the intercluster interactions, which can detach the assembled clusters and restrict the formation of ordered architectures. From a different view, the self-assembly of nanostructures can be understood as crystallization, which involves nucleation and growth. If the growth along one specific dimension is suppressed, 2D-oriented growth will be favored.[17–27] Most recently, CdSe NCs have been reported as intermediates for the synthesis of crystalline nanosheets.[8–13] Within the soft template of lamellar cadmium compounds, the 2D-limited recrystallization of NCs generates CdSe sheets.[9–11] Although this finding belongs to 2D colloidal synthesis, it opens the door to construct 2D architectures from preformed NCs.

Our basic idea was to extend the colloidal synthesis of crystalline nanosheets to construct self-assembled 2D architectures of NCs. As the most investigated model, Au NCs capped with hydrophobic alkylthiols were adopted to perform the 2D self-assembly in two miscible high-boiling-point solvents with a slight polarity difference. The microphase separation of the solvents creates a lamellar interface that acts as the soft template to direct Au cluster self-assembly into single-cluster-thick sheets by combining with intercluster hydrophobic–hydrophobic attraction (Figure 1).

The Au NCs employed for the self-assembled architectures are prepared in dibenzyl ether (BE) using 1-dodecanethiol (DT) to reduce Au^{III} at room temperature (Figure S1).

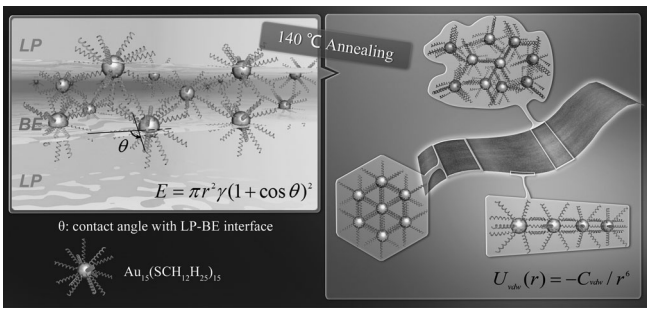

Figure 1. The self-assembly of Au_{15} into single-cluster-thick nanosheets by combining the surface tension at the LP–BE interface and intercluster hydrophobic attraction.

Simultaneously with the reduction of Au^{III} to Au^{I} and Au^{0}, didodecyl disulfide is generated as the byproduct.[28,29] Systematic characterization presents that the as-prepared Au clusters are Au_{15}, which are composed of $Au^{0}_{11}Au^{I}_{4}DT_{15}$ (Supporting Information, Figures S2–4). The Au_{15} clusters exhibit the average diameter of 1.5 ± 0.3 nm and a strong photoluminescence (PL) centered at 600 nm (Figure S2 a–d).

The self-assembly of Au_{15} clusters into diversified architectures is induced by adding liquid paraffin (LP) to the Au_{15} BE solution and annealing at 140 °C. For a typical nanosheet preparation, a Au_{15} solution (0.032 mmol) with a LP/BE volume ratio of 7.5:1 is heated to 140 °C and maintained for 1 h in vacuum (see the Supporting Information). Although such an operation does not alter the UV/Vis absorption and PL spectra, the fluorescence lifetime (Figures S2 and S5) and transmission electron microscopy (TEM) images reveal a change in morphology from isolated NCs to thin sheets comprised of clusters, with widths of ca. 300 nm and lengths of 200–1000 nm (Figure 2 b–d and Figure S2 a). High magnification TEM images confirm that the sheets are assemblies of individual clusters rather than crystalline Au (Figure 2 c, d). The distance between neighboring clusters is around 3.0 ± 0.3 nm, contributing both from the Au_{15} core and outside DT molecules. The length of DT in the elongated feature has been reported to be 1.7 nm.[30] Because the distance between Au_{15} cores is nearly the length of one DT, it indicates intercalation of DT between neighboring clusters.[31] On the basis of TEM observation, the angle of the DT alkyl chain at a tangent to the cluster surface is estimated to be 62°. Tapping mode atomic force microscopy (AFM) reveals that the thickness of the sheets is 1.68 nm (Figure 2 e), which is slightly larger than one Au_{15} core, but smaller than the distance between neighboring clusters in the sheets (Figure 2 d and Figure S2 a). This implies the preferential distribution of DT in the sheets. Furthermore,

[*] Z. N. Wu, C. W. Dong, H. X. Hao, Prof. H. Zhang, Prof. B. Yang
State Key Laboratory of Supramolecular Structure and Materials, College of Chemistry, Jilin University
Changchun 130012 (P. R. China)
E-mail: hao_zhang@jlu.edu.cn
Y. C. Li, Prof. Z. Y. Lu
State Key Laboratory of Theoretical and Computational Chemistry, Institute of Theoretical Chemistry, Jilin University
Changchun 130023 (P. R. China)
E-mail: luzhy@jlu.edu.cn

[**] This work was supported by the 973 Program of China (2009CB939701, 2012CB821500), NSFC (21174051, 21221063, 21025416, 91123031), and the Special Project from MOST of China.
Supporting information for this article is available on the WWW under http://dx.doi.org/10.1002/anie.201304122.

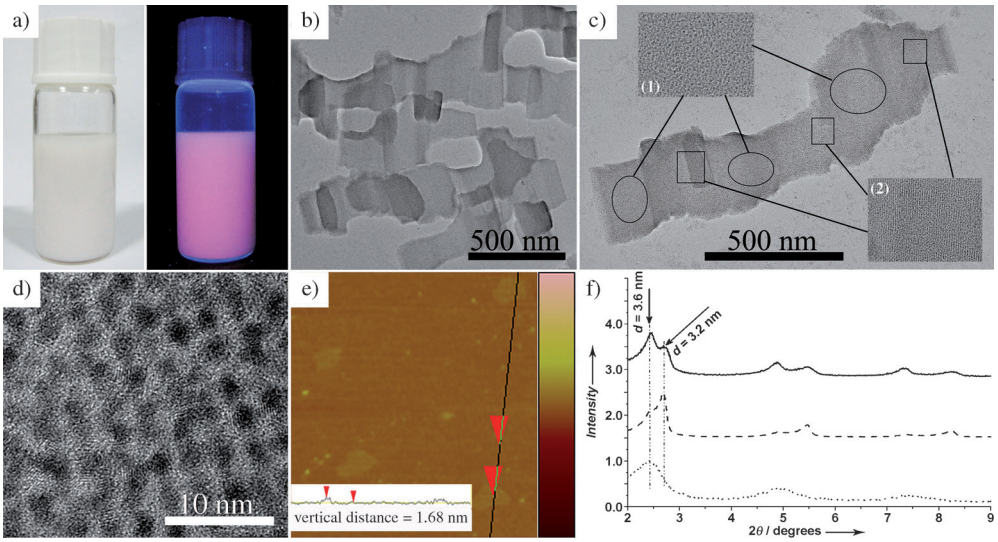

Figure 2. a) Optical (left) and PL (right) images of a $CHCl_3$ dispersion of the Au_{15} cluster nanosheets. b–d) TEM images of the adherent nanosheets at different magnifications. Inserts in (c): TEM images of the domains with disordered (1) and ordered (2) arrays of Au_{15}. e) Tapping-mode AFM and the corresponding topography cross section of the adherent nanosheets on a silica wafer. f) Small-angle region of the powder XRD patterns of the adherent nanosheets (——), isolated nanosheets (-----), and nanospheres (•••••). The corresponding TEM images are shown in (b) and Figure 3 a,d, respectively.

small-angle X-ray powder diffraction (XRD) presents peaks at 2.4 and 2.7°, which correspond to a *d* spacing of 3.6 nm and 3.2 nm, respectively (Figure 2 f); 2nd and 3rd order peaks are also observed at 4.9–5.5° and 7.3–8.3°. The appearance of two groups of XRD peaks indicates that two spatial characteristics of the clusters exist. By comparing with the XRD patterns of other Au_{15} self-assembled architectures (Figure 2 and Figure 3), it can be concluded that a *d* spacing of 3.6 nm relates to the alignment of Au_{15} clusters in the nanosheets, whereas a *d* spacing of 3.2 nm results from the stacking of nanosheets during XRD measurement (Figure S6). Although the *d* spacing from XRD is generally larger than that observed by TEM analysis, the results firmly support that the intra-nanosheet cluster distance is larger than the inter-nanosheets distance. This strongly suggests a preferential distribution of DT in the nanosheets.

The TEM images also reveal that the nanosheets are composed of interphase ordered and disordered domains (Figure 2 c insets), because the formation of the nanosheets involves step-wise assembly and reorganization in 2D (Figure S7). This is quite similar to the nucleation and 2D growth of semiconductor crystalline sheets.[10,11] Under heating, solvent evaporation enhances the local concentration of Au_{15} clusters and thereby leads to aggregation-nucleation. In our system, two miscible solvents, LP and BE, with only a slight polarity difference, are employed.[32] The Au_{15} clusters are more compatible with BE than LP, because of the higher polarity of BE. So, the aggregation-nucleation mainly occurs in the BE-rich domain (Figure 1). It is reasonable to consider that the generation of nanosheets relates to the total volume and LP/BE ratio variation during annealing. Density and refractive index measurements indicate that the LP/BE ratio is constant before and after 140 °C annealing (Figure S8). However, a slight volume decrease from 17.4 mL to 17.1 mL was found (Table S1), owing to the application of vacuum. The decrease in solvent volume enhances the local concentration of Au_{15} clusters, facilitating the aggregation-nucleation. Note that the aforementioned nanosheets are formed from the adherent aggregates (Figure 2 and S7). We considered controlling the evolution of the self-assembled architectures by tuning the evaporation rate of solvents. In this scenario, N_2 was used rather than vacuum, to lower the evaporation rate. This leads to differential solvent loss (Table S1), thus avoiding further aggregation after nucleation and producing

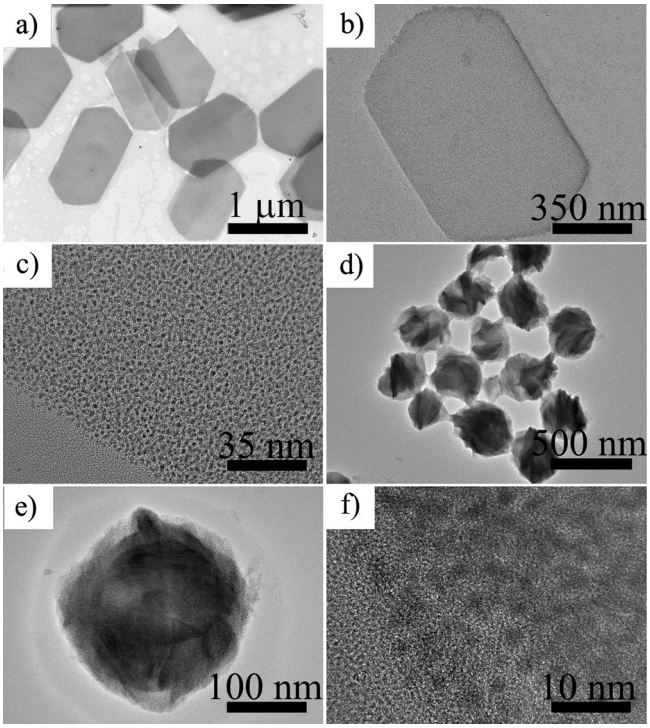

Figure 3. Low (a) and high (b and c) magnification TEM images of the isolated nanosheets, produced by annealing the Au_{15} cluster solution at 140 °C for 10 min under N_2. The cluster concentration is 0.032 mmol. Low (d) and high (e and f) magnification TEM images of the nanospheres obtained by annealing the Au_{15} solution at 140 °C for 1 h under vacuum. The cluster concentration is 0.008 mmol. The LP/BE volume ratio is 7.5:1.

isolated nanosheets with uniform size and shape (Figure 3a–c).

The 2D self-assembly must be carried out at high Au_{15} concentration (Figure 3d–f and Figure S9). As the concentration decreases from 0.032 mmol to 0.008 mmol, the self-assembled architectures turn from sheets into spheres, although the spheres still maintain the size and spectral properties of the original Au_{15} clusters (Figure 3f and Figure S10). When the concentration decreases to 0.002 mmol, the nanospheres disappear and irregular aggregates form. Temporal evolution of the self-assembled architectures further indicates that the concentration greatly influences the morphologies of aggregated clusters (Figures S7 and S11), namely the intermediates, making the subsequent self-assembly follow a different pathway. The apparent disparity in cluster aggregation also reflects the different status of the binary solvents, because of the different solubility of the clusters in LP and BE.

This consideration is further revealed by the effect of LP/BE volume ratio on the morphologies of self-assembled architectures (Figure S12). As the initial LP/BE ratio decreases, the morphologies turn from nanosheets to bipyramids and finally to irregular aggregates. At low concentration (such as 0.008 mmol), the morphologies also depend on the LP/BE ratio (Figure S13). Although LP and BE are miscible, there exists a microphase separation and thus an interface between LP and BE at higher temperatures (Figure S14), which acts as a soft template to direct Au_{15} self-assembly. A high LP/BE ratio is thought to generate lamellar structures, allowing 2D Au_{15} assembly.

For a better understanding of the self-assembly mechanism, we performed a dissipative particle dynamics (DPD) simulation using a coarse-grained (CG) model.[33,34] The corresponding results are summarized in a phase diagram (Figure S15). To map these experimental systems, we choose an appropriate coarse-graining level for BE, LP, DT, and Au (Table S2). Our DPD simulation is in good agreement with experimental observations. Namely, that the formation of the lamellar microphase is favored at high LP/BE ratio and high Au_{15} concentration; otherwise, the self-assembled architectures undergo a transition from nanosheets to bipyramids, nanospheres, and irregular aggregates (Figure S9, S12, and S13). When several Au_{15} clusters approach each other, the DT chains can accommodate new configurations and allow redistribution on the Au_{15} surface. At higher LP/BE ratios, the Au_{15} clusters are even more compatible with BE. The surface energy (E) of Au clusters at the LP–BE interface can be estimated according to the contact angle with LP or BE (Figure 1), where r is the radius of Au clusters, γ is the interfacial tension between BE and LP, θ is the contact angle of the Au clusters with LP that is larger than 90°.[35] It means that it is energetically favorable for Au clusters to remain in BE, which promotes cluster aggregation and the generation of nanosheets.

The formation of nanosheets must break through a temperature barrier, which was found to be 140 °C in our experiments. In this context, the Au clusters are capped with DT. Similar to the most examples of self-assembled architectures from hydrophobic nanostructures,[10] the intercalation of the DT alkyl chains permits the self-assembly of Au_{15} clusters by hydrophobic attraction. However, the thermodynamically allowed self-assembly should cross the energy barrier.[31] The longer alkyl chains contribute to stronger hydrophobic attraction, but require higher temperature to cross the barrier. Thus, annealing at 140 °C is necessary to enhance alkyl chain mobility and thereby facilitate Au_{15} cluster assembly. In our experiment, the turbid nanosheet solution turns clear when the temperature is slightly higher than 140 °C (Figure S16), thus showing the high mobility of the DT alkyl chain over the temperature barrier. The hydrophobic attraction between DT is strong, represented by the capability to drive DT distribution in the nanosheets (Figure 2d–f). The hydrophobic attraction between the neighboring Au_{15} clusters is calculated to be $7 k_B T$ (Figure S17), where k_B is the Boltzmann constant and T is the absolute temperature. In addition, ^{1}H NMR and mass spectra demonstrate the coexistence of didodecyl disulfides in the nanosheets (Figure S18 and S19). As didodecyl disulfides possess longer alkyl chains than DT, it may assist the formation of nanoarchitectures by supplying additional hydrophobic attraction. We do not exclude the existence of intercluster static, dipolar, and van der Waals interactions. However, for hydrophobic Au_{15} clusters with very small size, these interactions are negligible in comparison with the thermal fluctuation energy, $k_B T$, thus they contribute less to the 2D self-assembly process.[36]

Most importantly, strong hydrophobic attraction leads to a reorganization of the aggregated clusters at 140 °C and finally produces nanosheets. Such reorganization includes two aspects: First, the isotropic hydrophobic attraction between neighboring NCs combines with the surface tension at the LP–BE interface, which generates a strong tension with a 2D orientation (Figure 1). This drives the 2D reorganization of aggregated clusters during annealing. As a result, single-cluster-thick sheets are produced. Second, at the boundaries of the adherent aggregates, the clusters are less limited by the neighboring ones. This leads to the ordered alignment of Au_{15} clusters. In contrast, the clusters in the aggregates are greatly limited, and thus remain unordered (Figure 2c). For the system with a lower solvent-evaporation rate (Figure 3a–c), the less dynamic alkyl chains of DT facilitate the reorganization of NCs in the aggregates, but suppresses the adherence of the aggregates. Consequently, isolated nanosheets are produced rather than adherent ones. Because of the less dynamic alkyl chains, the alignment of clusters is disordered (Figure 3c).

The 2D self-assembly of Au_{15} clusters is not limited to mixtures of LP and BE. Nanosheets are also produced in a binary system of octadecene (ODE) and BE (Figure S20). Because the polarity of ODE is closer to BE than LP,[32] more ODE is required for generating the lamellar microphase and enough surface tension to direct the self-assembly.

In summary, we demonstrate the self-assembly of DT-capped Au_{15} clusters into single-cluster-thick nanosheets in high-boiling solvents. The trick is to anneal the clusters in two miscible solvents with a slight polarity difference. The solvent microphase separation generates a lamellar interface, which acts as a soft template to direct the 2D self-assembly. In this

scenario, the surface tension of the interface combines with the isotropic hydrophobic attraction between the neighboring clusters, thus generating the driving force for 2D orientation. The formation of nanosheets relates to both cluster aggregation (nucleation) and reorganization (recrystallization) at the interface. Consequently, the morphologies of the self-assembled architectures are adjustable by altering cluster concentration, solvent volume ratio, and the differential volume variation of the solvents. Because the as-prepared nanosheets are dispersible in common organic solvents such as chloroform, they will be promising building blocks for the design of ultrathin devices through solution processing.

Received: May 14, 2013
Published online: August 27, 2013

Keywords: gold · hydrophobic attraction · interfaces · nanostructures · self-assembly

[1] S. Ithurria, M. D. Tessier, B. Mahler, R. P. S. M. Lobo, B. Dubertret, A. L. Efros, *Nat. Mater.* **2011**, *10*, 936 – 941.
[2] Z. Y. Tang, Z. L. Zhang, Y. Wang, S. C. Glotzer, N. A. Kotov, *Science* **2006**, *314*, 274 – 278.
[3] J. H. Yu, X. Y. Liu, K. E. Kweon, J. Joo, J. Park, K. T. Ko, D. W. Lee, S. P. Shen, K. Tivakornsasithorn, J. S. Son, J. H. Park, Y. W. Kim, G. S. Hwang, M. Dobrowolska, J. K. Furdyna, T. Hyeon, *Nat. Mater.* **2010**, *9*, 47 – 53.
[4] S. Z. Butler, S. M. Hollen, L. Y. Cao, Y. Cui, J. A. Gupta, H. R. Gutiérrez, T. F. Heinz, S. S. Hong, J. X. Huang, A. F. Ismach, E. Johnston-Halperin, M. Kuno, V. V. Plashnitsa, R. D. Robinson, R. S. Ruoff, S. Salahuddin, J. Shan, L. Shi, M. G. Spencer, M. Terrones, W. Windl, J. E. Goldberger, *ACS Nano* **2013**, *7*, 2898 – 2926.
[5] Y. Xia, T. D. Nguyen, M. Yang, B. Lee, A. Santos, P. Podsiadlo, Z. Tang, S. C. Glotzer, N. A. Kotov, *Nat. Nanotechnol.* **2011**, *6*, 580 – 587.
[6] J. Gong, G. Li, Z. Tang, *Nano Today* **2012**, *7*, 564 – 585.
[7] M. Grzelczak, J. Vermant, E. M. Furst, L. M. Liz-Marzán, *ACS Nano* **2010**, *4*, 3591 – 3605.
[8] Y. Y. Wang, Y. H. Liu, Y. Zhang, F. D. Wang, P. J. Kowalski, H. W. Rohrs, R. A. Loomis, M. L. Gross, W. E. Buhro, *Angew. Chem.* **2012**, *124*, 6258 – 6261; *Angew. Chem. Int. Ed.* **2012**, *51*, 6154 – 6157.
[9] J. S. Son, X. D. Wen, J. Joo, J. Chae, S.-I. Baek, K. Park, J. H. Kim, K. An, J. H. Yu, S. G. Kwon, S. H. Choi, Z. W. Wang, Y. W. Kim, Y. Kuk, R. Hoffmann, T. Hyeon, *Angew. Chem.* **2009**, *121*, 6993 – 6996; *Angew. Chem. Int. Ed.* **2009**, *48*, 6861 – 6864.
[10] J. Yang, J. S. Son, J. H. Yu, J. Joo, T. Hyeon, *Chem. Mater.* **2013**, *25*, 1190 – 1198.
[11] Y. H. Liu, F. D. Wang, Y. Y. Wang, P. C. Gibbons, W. E. Buhro, *J. Am. Chem. Soc.* **2011**, *133*, 17005 – 17013.
[12] C. Bouet, M. D. Tessier, S. Ithurria, B. Mahler, B. Nadal, B. Dubertret, *Chem. Mater.* **2013**, *25*, 1262 – 1271.
[13] S. Ithurria, G. Bousquet, B. Dubertret, *J. Am. Chem. Soc.* **2011**, *133*, 3070 – 3077.
[14] H. J. Yin, H. J. Tang, D. Wang, Y. Gao, Z. Y. Tang, *ACS Nano* **2012**, *6*, 8288 – 8297.
[15] L. Li, Q. B. Wang, *ACS Nano* **2013**, *7*, 3053 – 3060.
[16] H. Thérien-Aubin, Z. L. Wu, Z. H. Nie, E. Kumacheva, *J. Am. Chem. Soc.* **2013**, *135*, 4834 – 4839.
[17] P. Geiregat, Y. Justo, S. Abe, S. Flamee, Z. Hens, *ACS Nano* **2013**, *7*, 987 – 993.
[18] X. D. Zhang, J. J. Zhang, J. Y. Zhao, B. C. Pan, M. G. Kong, J. Chen, Y. Xie, *J. Am. Chem. Soc.* **2012**, *134*, 11908 – 11911.
[19] I. T. Sines, D. D. Vaughn, A. J. Biacchi, C. E. Kingsley, E. J. Popczum, *Chem. Mater.* **2012**, *24*, 3088 – 3093.
[20] S. Acharya, S. Sarkar, N. Pradhan, *J. Phys. Chem. Lett.* **2012**, *3*, 3812 – 3817.
[21] S. Acharya, M. Dutta, S. Sarkar, D. Basak, S. Chakraborty, N. Pradhan, *Chem. Mater.* **2012**, *24*, 1779 – 1785.
[22] N. F. Zheng, X. H. Bu, J. Lauda, P. Y. Feng, *Chem. Mater.* **2006**, *18*, 4307 – 4311.
[23] K. Akatsuka, M.-A. Haga, Y. Ebina, M. Osada, K. Fukuda, T. Sasaki, *ACS Nano* **2009**, *3*, 1097 – 1106.
[24] C. Xu, Y. Zeng, X. H. Rui, N. Xiao, J. X. Zhu, W. Y. Zhang, J. Chen, W. L. Liu, H. T. Tan, H. H. Hng, Q. Y. Yan, *ACS Nano* **2012**, *6*, 4713 – 4721.
[25] Z. Li, X. G. Peng, *J. Am. Chem. Soc.* **2011**, *133*, 6578 – 6586.
[26] S. Ithurria, B. Dubertret, *J. Am. Chem. Soc.* **2008**, *130*, 16504 – 16505.
[27] C. Bouet, B. Mahler, B. Nadal, B. Abecassis, M. D. Tessier, S. Ithurria, X. Z. Xu, B. Dubertret, *Chem. Mater.* **2013**, *25*, 639 – 645.
[28] Y. Yu, X. Chen, Q. F. Yao, Y. Yu, N. Yan, J. P. Xie, *Chem. Mater.* **2013**, *25*, 946 – 952.
[29] A. S. Susha, M. Ringler, A. Ohlinger, M. Paderi, N. LiPira, G. Carotenuto, A. L. Rogach, J. Feldmann, *Chem. Mater.* **2008**, *20*, 6169 – 6175.
[30] F. K. Wang, X. H. Zhang, Z. Zhang, C. B. He, *J. Mater. Chem.* **2011**, *21*, 15167 – 15170.
[31] H. Y. Fan, E. Leve, J. Gabaldon, A. Wright, R. E. Haddad, C. J. Brinker, *Adv. Mater.* **2005**, *17*, 2587 – 2590.
[32] The dielectric constants of LP, ODE, and BE are 2.0, 2.2, and 3.8, respectively.
[33] H. J. Qian, Z. Y. Lu, L. J. Chen, Z. S. Li, C. C. Sun, *Macromolecules* **2005**, *38*, 1395 – 1401.
[34] I. C. Pons-Siepermann, S. C. Glotzer, *ACS Nano* **2012**, *6*, 3919 – 3924.
[35] H. W. Duan, D. Y. Wang, D. G. Kurth, H. Möhwald, *Angew. Chem.* **2004**, *116*, 5757 – 5760; *Angew. Chem. Int. Ed.* **2004**, *43*, 5639 – 5642.
[36] K. J. M. Bishop, C. E. Wilmer, S. Soh, B. A. Grzybowski, *Small* **2009**, *5*, 1600 – 1630.

